

# Recent progress in the upgrade of the TCV EC-system with two 1MW/2s dual-frequency (84/126GHz) gyrotrons

Stefano Alberti<sup>1,\*</sup>, Jérémy Genoud<sup>1</sup>, Timothy Goodman<sup>1</sup>, Jean-Philippe Hogge<sup>1</sup>, Laurie Porte<sup>1</sup>, Miguel Silva<sup>1</sup>, Trach-Minh Tran<sup>1</sup>, Minh-Quang Tran<sup>1</sup>, Konstantinos Avramidis<sup>2</sup>, Ioannis Pagonakis<sup>2</sup>, Jianbo Jin<sup>2</sup>, Stefan Illy<sup>2</sup>, Gerd Gantenbein<sup>2</sup>, John Jelonnek<sup>2</sup>, Manfred Thumm<sup>2</sup>, William Bin<sup>3</sup>, Alex Bruschi<sup>3</sup>, Saul Garavaglia<sup>3</sup>, Alessandro Moro<sup>3</sup>, Walter Kasparek<sup>4</sup>, François Legrand<sup>5</sup>, Etienne Perial<sup>5</sup>, Yoan Rozier, Fabio Cismondi<sup>6</sup>, Niek Doelman<sup>7</sup>

<sup>1</sup>Ecole Polytechnique Fédérale de Lausanne (EPFL), SPC, CH-1015, Lausanne, Switzerland

<sup>2</sup>IHM, Karlsruhe Institute of Technology (KIT), Kaiserstrasse 12, D-76131, Karlsruhe, Germany

<sup>3</sup>Institute of Plasma Physics “P. Caldirola”, National Research Council of Italy, Milano, Italy

<sup>4</sup>Institute for Interfacial Process Engineering and Plasma Technology, University of Stuttgart, D-70569 Stuttgart, Germany

<sup>5</sup>Thales Electron Devices, Vélizy-Villacoublay, France

<sup>6</sup>PPPT Power Plant Physics and Technology EUROfusion, D-85748 Garching, Germany

<sup>7</sup>Department of OptoMechatronics, TNO Technical Sciences, NL-2600 AD, Delft, The Netherlands

**Abstract.** The upgrade of the EC-system of the TCV tokamak has entered in its realization phase and is part of a broader upgrade of TCV. The MW-class dual-frequency gyrotrons (84 or 126GHz/2s/1MW) are presently being manufactured by Thales Electron Devices with the first gyrotron foreseen to be delivered at SPC by the end of 2017. In parallel to the gyrotron development, for extending the level of operational flexibility of the TCV EC-system the integration of the dual-frequency gyrotrons adds a significant complexity in the evacuated 63.5mm-diameter HE<sub>11</sub> transmission line system connected to the various TCV low-field side and top launchers. As discussed in [1], an important part of the present TCV-upgrade consists in inserting a modular closed divertor chamber. This will have an impact on the X3 top-launcher which will have to be reduced in size. For using the new compact launcher we are considering employing a Fast Directional Switch (FADIS), combining the two 1MW/126GHz/2s rf-beams into a single 2MW rf-beam.

## 1 Introduction

TCV is presently undergoing major heating upgrades [1], with the installation of a neutral beam for direct ion heating and increasing the EC power injected in X-mode at the third harmonic (X3-upgrade). The neutral beam, with energies of 20-35keV and power up to 1MW for 2s, is operational since spring 2016 and a second neutral beam with higher energy (50-60keV, 1MW, 2s) is foreseen in 2018. The so called X3-upgrade project consists of adding two dual-frequency gyrotrons (126 GHz/84 GHz) with a total power at 126 GHz (for top-launch X3) or at 84 GHz (for low field side (LFS) injection X2) of 2MW. The three existing gyrotrons used for X3-ECH and operating at 118 GHz will be relocated to inject power from the LFS using the existing X2 transmission lines and launchers.

The heating upgrade will give access to plasma regimes and configurations with high normalized plasma pressure and wide range of temperature ratios, including  $T_e/T_i \sim 1$ . As shown in Fig. 1, which is obtained from an ASTRA simulation [2] of a standard TCV configuration, to approach the ITER relevant range of normalized  $\beta_N$  values ( $\beta_N \sim 2-2.5$ ), X3 power levels higher than the presently available 1.5MW are necessary. Considering the X3-upgrade with 2MW of additional power (total 3.5MW) and 1MW of Neutral Beam Injection NBI, the simulations show that, for the reference discharge described in Fig.1, central electron and ion temperatures as high as  $T_e(0)=4\text{keV}$  and  $T_i(0)=2.5\text{keV}$  can be reached.

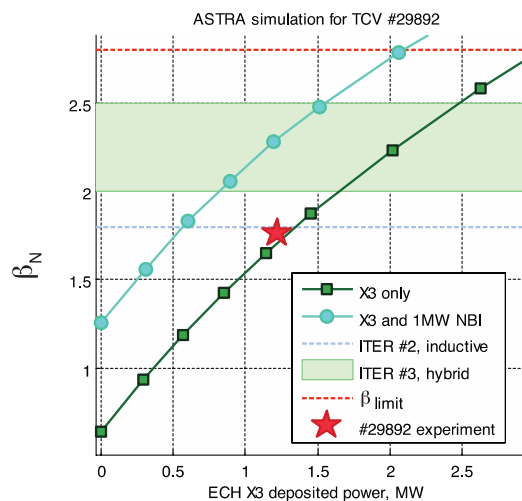


**Fig. 1.** ASTRA simulation of the TCV plasma performance as a function of X3 absorbed power based on an actual scenario (H-mode discharge 29892, with  $I_p=410\text{kA}$ ,  $B_T=1.44\text{T}$ ,  $Z_{\text{eff}}=2.6$ ,  $n_e(0)=6.5 \times 10^{19}\text{m}^{-3}$ ,  $T_e(0)=2.8\text{keV}$ ,  $T_i(0)=0.9\text{keV}$ ,  $q_{95}=2.5$ ; the shaping parameters are  $\kappa_{95}=1.68$  and  $\delta_{95}=0.36$ ).

## 2 X3 Single-pass absorption properties

As shown in Fig.2, for the central electron temperature and density given in Fig.1, TORAY[3] simulations

\* Corresponding author: [stefano.alberti@epfl.ch](mailto:stefano.alberti@epfl.ch)

predict a single-pass absorption in excess of 80% with X3 top-launch. This absorption level has been experimentally confirmed in the past [4]. Based on these results and the ASTRA simulations, including the 1MW NBH, full single-pass absorption in H-mode plasmas will then be ensured with the 2MW/126GHz injected from the top launcher. With the efficient electron bulk heating using the top-launch, single pass absorption well exceeding 70% is to be expected when injecting the 1.5MW/118GHz rf-power for X3 heating from the low-field side. This will enable localized power deposition necessary for MHD control. The ECCD efficiency for the X3 injected power from the LFS is negligible.

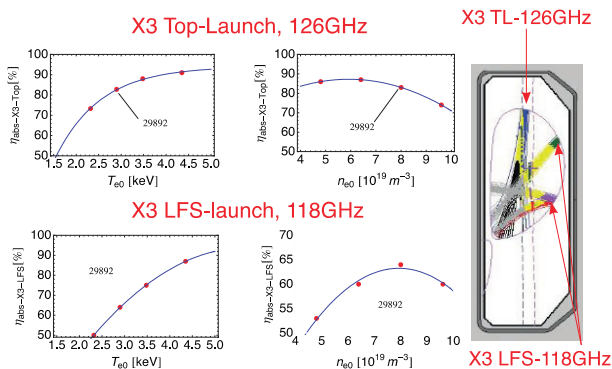


**Fig. 2.** TORAY simulations of the single-pass absorption for the X3 top-launch @126GHz (TL) and the X3 LFS-launch @118GHz versus central electron temperature and density. The decrease of the absorption at high density is due to the density dependence of the optical-depth via the index of refraction. The reference plasma parameters for discharge 29892 are given in Fig. 1.

As discussed later on (see Fig. 6), when the new dual-frequency gyrotron will be operational, the transmission lines of the three 118GHz gyrotron will be reconfigured for low-field side injection using the existing X2 launchers. This configuration has been used and validated during the first X3 heating experiments [5].

### 3 Dual-frequency gyrotron

The gyrotron design is essentially based on modifications of the W7-X gyrotron [6-8] in which some sub-components have been redesigned (see Fig. 3 [9]) using the most advanced models.

The electron beam operating parameters have been chosen to be compatible with the existing HV power supplies, and the magnetic field profile provided by the W7-X gyrotron magnets has been rescaled for an operation at 84GHz and 126GHz. The operating modes have been chosen such that their coupling to the electron beam is close to optimal, with frequencies (84GHz and 126GHz) as close as possible to those presently used on the TCV ECH system (82.7GHz and 118GHz), with the additional constraint that their wavelengths should correspond to an integer number of half-wavelengths in the gyrotron CVD diamond window. This resulted in the

choice of the modes TE<sub>17,5</sub> at 83.91GHz and TE<sub>26,7</sub> at 126.16GHz respectively.

The main redesigned component is the electron gun for which, instead of a diode gun (W7-X), a triode gun will be implemented, providing flexibility in the range of achievable electron beam parameters at both frequencies.

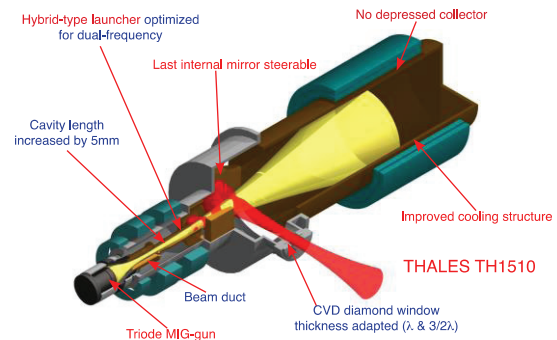


**Fig. 3.** Schematic of the dual-frequency gyrotron (TH1510) manufactured by Thales Electron Devices. Indicated are the parts which have been redesigned from the TH1507 (140GHz, W7-X) with highlighted in red the major redesigned components.

Recent design criteria such as the absence of potential wells and the avoidance of trapped electrons emitted from any part of the gun have been considered in the gun design [10].

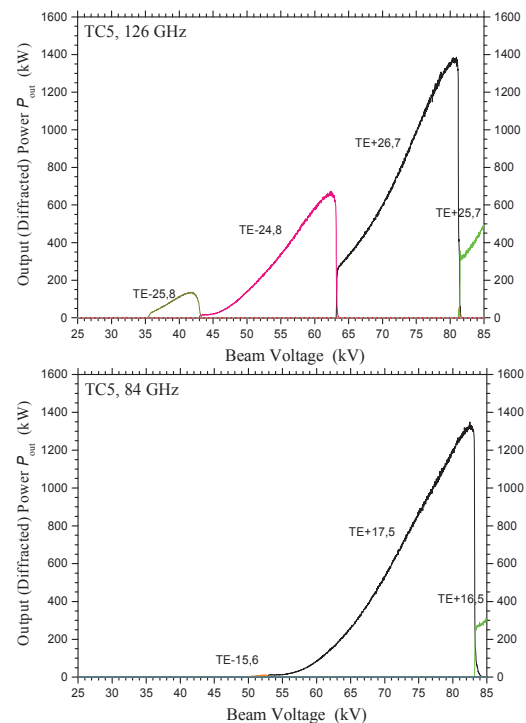


**Fig. 4.** EURIDICE[11] multimode simulations including the time dependence of the beam parameters and a 16% rms spread in the electron beam velocity ratio. The beam current is 40A and the pitch factor is 1.3 in both cases. Top: mode TE<sub>26,7</sub> @ 126GHz. Bottom: mode TE<sub>17,5</sub> @ 84GHz.

The gyrotron cavity underwent a very minor redesign essentially consisting in lengthening by 5mm the

constant radius section in order to increase the quality factor and the efficiency at frequencies lower than the original one (140GHz). Monomode and multi-mode time-dependent simulations were carried out to validate the mode choices and perform a fine tuning of the magnetic field. As shown in Fig. 4, single-mode operation with a diffracted power in excess of 1MW at the operating voltage (78kV) is predicted at both frequencies, with a stability range of 2-4 kV.

In order to reach the highest Gaussian mode content, a significant effort has been placed in the redesign and optimisation of the launcher and the internal mirrors [12]. A satisfying compromise between the Gaussian content, the beam size and centering at the window and the beam waist location could be found and is illustrated on Fig. 5, where the field distribution for the mode  $TE_{26,7}$  is shown with a linear scale. The beam waist is of the order of 20mm and is located approximately 100mm after the window. The results were cross-checked with SURF3D[13], which additionally estimated the stray radiation level to < 4%. The gyrotron design parameters are summarized in Table 1.

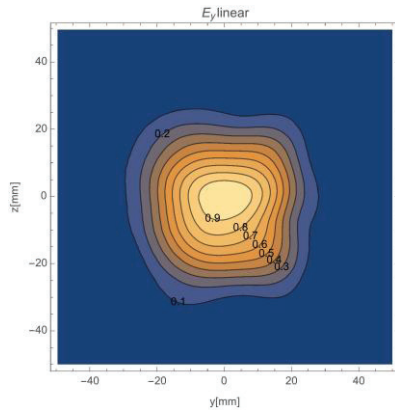


**Fig. 5.** Normalized electric field distribution at the window (linear scale), mode  $TE_{26,7}$ . The estimated Gaussian content is 97.6% and the stray radiation level is estimated at 2.5%.

Based on the fact that on TCV only 2s rf-pulses will be used, together with the constraint of using the existing high-voltage power supplies, it has been shown, using advanced thermo-hydraulic simulation models, that the collector loading allows the operation without a depressed collector. Compared to the W7-X gyrotron, and based on the simulations an improved cooling structure in the collector region has been implemented.

**Table 1.** Dual-frequency gyrotron design parameters[14].

Operating cavity mode	$TE_{17,5}$	$TE_{26,7}$
Frequency [GHz]	83.91	126.16
RF output power [MW]	1.05	1.2
Cavity wall-loading [ $kW/cm^2$ ]	1.1	2.1
Beam current [A]	40	40
Beam energy [keV]	78	78
Mod-anode voltage [kV]	-38	-26
Pitch angle, $\alpha$	$\sim 1.3$	$\sim 1.3$
Cavity magnetic field, [T]	3.31	4.98
Electronic efficiency [%]	35	41
Gaussian content [%]	97.7	97.6

The two gyrotrons (TH1510) are being manufactured by the French company Thales Electron Devices, with the first unit foreseen to be operational on TCV in the first half of 2018. In parallel to the gyrotron manufacturing, two cryogen-free superconducting magnets are being procured from the American company Cryomagnetics. Apart from the cryogen-free aspect, the magnet design is based on the superconducting magnets used for the gyrotrons at W7-X.

## 4 System Implementation

In parallel to the gyrotron development, for extending the level of operational capability of the TCV EC-system, the integration of the dual-frequency gyrotrons adds a significant complexity in the evacuated 63.5mm-diameter  $HE_{11}$  transmission line transporting the rf-power from the gyrotrons to the various TCV low-field side and top launchers. Fig. 6 shows the layout of the upgraded EC-system.

The two dual-frequency gyrotrons will be connected to their respective evacuated Matching Optics Units (MOU) which will contain the quadratic surface-contour function optics for maximizing the coupling to the  $HE_{11}$  waveguides (63.5mm internal diameter) for each frequency. The first mirror after the gyrotron window will be movable under vacuum for redirecting the rf-beam towards the corresponding mirrors set for each frequency, 84 or 126GHz. Each mirror set consists of two fixed mirrors. With this design the MOU also plays the role of a high-power evacuated rf-switch. The two MOU outputs will be connected to the corresponding  $HE_{11}$  transmission lines manufactured by General Atomics (GA).

The rf-wave polarization control will be performed at the transmission line miter bends. For the two lines transmitting the 84GHz frequency and connected to low-field side launchers, real-time full-polarization control will be possible by using two sets of remotely controlled miter bend pairs. For the two lines transmitting the 126GHz and connected to the top-launcher only the linear polarization needs to be controlled which will be realized via a single non-motorized miter bend on each line.

With the redirection of the 118GHz power toward the low-field side launchers, these LFS launchers will be each launching either 82.7GHz(0.5MW/2s) or, alternatively, 84GHz(1MW/2s) or 118GHz(0.5MW/2s). This flexibility is realized by using rotary switches with three inputs and one output. All the transmission line components will be procured from GA and integrated into the existing system purchased from GA in the period 2000-2005.

As discussed in [1], a further upgrade of TCV consists in inserting a modular closed divertor chamber [15]. This will have an impact on the X3 top-launcher which will have to be reduced in size with the aim of rendering this system mountable and dismountable on a significantly shorter time scale than in the present situation. For using the new compact launcher we are considering to employ a Fast Directional Switch [16]

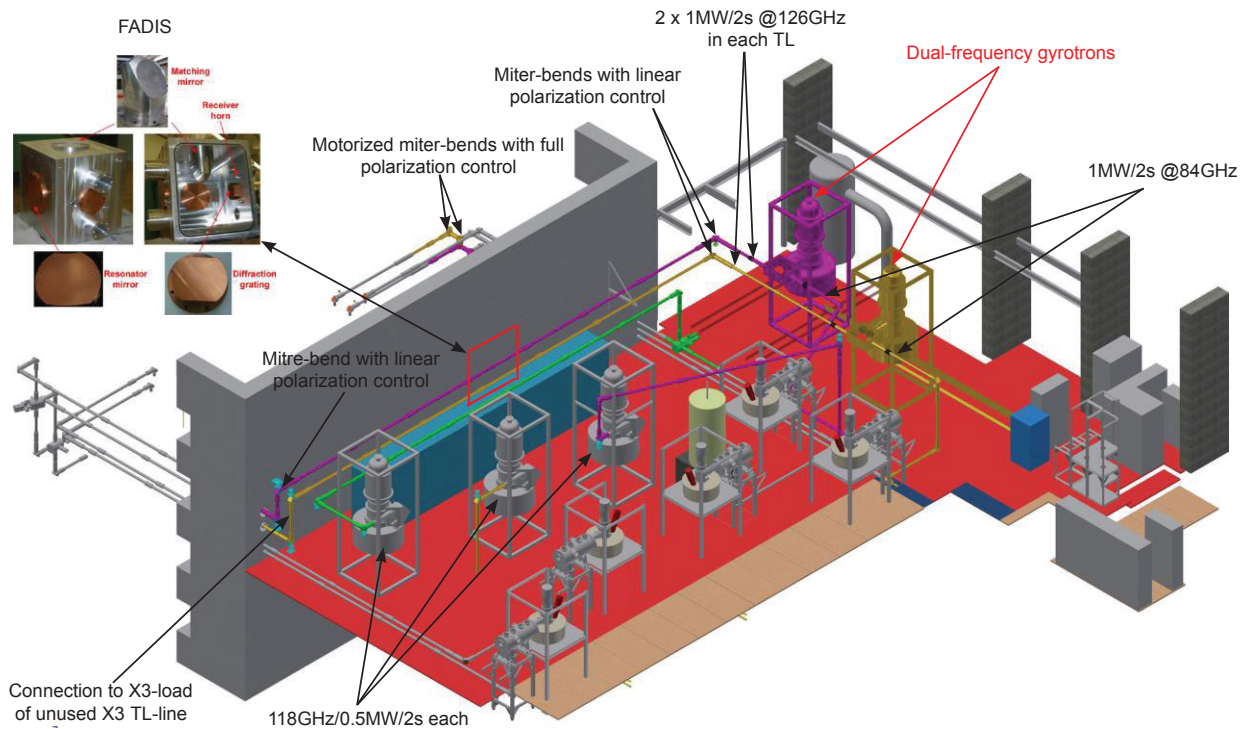


**Fig. 6.** Layout of the upgraded TCV EC-system. The envisaged position of the FADIS is indicated by the red square “traversed” by the two 126GHz transmission lines. In the inset, an example of the FADIS vacuum-vessel and some internal components are shown. The 5 gyrotrons, without labels, in the lower part of the figure are 82.7GHz gyrotrons used for X2-ECH/ECCD.

(FADIS), combining the two 1MW/126GHz/2s rf-beams into a single 2MW rf-beam. As schematically shown in Fig. 6, the FADIS will be placed in the region of the long-leg straight 126GHz transmission line section. One output of the FADIS will be connected to the compact X3 top-launcher, whereas the second output will be connected to an existing rf-power load. For the FADIS resonant-channel, a feedback-controlled mirror drive tracks the diplexer resonance [17] according to the gyrotron frequency chirp which is expected to shift by approximately 300-400MHz over typically the first 500ms of the gyrotron pulse. This frequency chirp is a consequence of the thermally induced gyrotron cavity expansion and, considering that the maximum pulse-length in TCV is of 2s, it is important that the mirror feedback-control locks to the gyrotron frequency on a time scale significantly shorter than the cavity thermal time constant. The first tests of the FADIS in ITER relevant conditions are foreseen for the end of 2018.

In conclusion, the additional power generated by the two dual-frequency gyrotrons will complete and maintain the heating capabilities on TCV in view of regimes of increased relevance for burning plasma conditions. The TCV multi-gyrotron system together with the complex transmission line system, including the FADIS, is an ideal test-bed for further validating ITER relevant EC-technology.

Work supported by the Ecole Polytechnique Fédérale de Lausanne (EPFL).

## References

1. A. Fasoli et al., Nucl. Fusion **55**(4), 043006 (2015).
2. G. Pereverzev et al., ASTRA. Automated System for Transport Analysis in a Tokamak, (Max-Planck Institute for Plasma Physics, Garching, IPP) Report 5/98 (2002).
3. K. Matsuda, IEEE Trans. Plasma Sci. **17**, 6 (1989)
4. L. Porte et al., Nucl. Fusion **47**(8), 952 (2007)
5. S. Alberti et al., Nucl. Fusion **42**(1), 42 (2002)
6. S. Alberti et al., Fusion Engineering and Design **53**, 387 (2001)
7. M. Thumm et al., IEEE Trans. on Plasma Science, **35**(2), 143 (2007).
8. J. Jelonnek et al., IEEE Trans. on Plasma Science, **42**(5), 1135 (2014).
9. S. Alberti et al., Proc. 41<sup>st</sup> IRMMW-THz Conf., Copenhagen (2016), W2E4 - 3134041
10. I. Pagonakis et al., Phys. Plasmas **23**, 023105 (2016)
11. K.A. Avramides et al., Proc. of the 17th Joint Workshop on Electron Cyclotron Emission and Electron Cyclotron Resonance Heating, Deurne, The Netherlands, 7-11 May 2012, EPJ Web of Conferences **32**, 04016 (2012).
12. J. Jianbo et al., IEEE Trans. on MTT, **65**(3), 699 (2017)
13. J. Neilson, Proc. 29<sup>th</sup> IRMMW-THz Conf., Karlsruhe p. 667-668 (2004),
14. J.-Ph. Hogge. et al., Proc. 40<sup>th</sup> IRMMW-THz Conf., Hong-Kong (2015), W2E4 - 3134041
15. H. Reimerdes et al., Nucl. Materials and Energy, (2017) <http://dx.doi.org/10.1016/j.nme.2017.02.013>
16. W. Kasperek et al., Nucl. Fusion **48**, 054010 (2008)
17. W. Kasperek et al., Nucl. Fusion **56**, 126001 (2016)